Evidence for a Millisecond Pulsar in 4U 1636-53 During a Superburst

Tod E. Strohmayer, and Craig. B. Markwardt[1]

Laboratory for High Energy Astrophysics, NASA's Goddard Space Flight Center, Greenbelt, MD 20771; stroh@clarence.gsfc.nasa.gov, craigm@milkyway.gsfc.nasa.gov

[1]*also, Dept. of Astronomy, University of Maryland, College Park, MD 20742*

ABSTRACT

We report the discovery with the Proportional Counter Array on board the Rossi X-ray Timing Explorer of highly coherent $\sim$ 582 Hz pulsations during the February 22, 2001 (UT) "superburst" from 4U 1636-53. The pulsations are detected during an $\sim$ 800 s interval spanning the flux maximum of the burst. Within this interval the barycentric oscillation frequency increases in a monotonic fashion from $\sim$ 581.89 to 581.93 Hz. The predicted orbital motion of the neutron star during this interval is consistent with such an increase as long as optical maximum corresponds roughly with superior conjunction of V801 Arae, the optical companion to the neutron star in 4U 1636-53. We show that a range of circular orbits with $90 < v_{ns} \sin i < 175$ km s^{-1} and $0.336 > \phi_0 > 0.277$ for the neutron star can provide an excellent description of the frequency and phase evolution. The brevity of the observed pulse train with respect to the 3.8 hour orbital period unfortunately does not allow more precise constraints. The average pulse profile is sinusoidal and the time averaged pulsation amplitude, as inferred from the half amplitude of the sinusoid is 1%, smaller than typical for burst oscillations observed in normal thermonuclear bursts. We do not detect any higher harmonics nor the putative subharmonic near 290 Hz. The 90% upper limits on signal amplitude at the subharmonic and first harmonic are 0.1 and 0.06%, respectively. The highly coherent pulsation, with a $Q \equiv \nu_0/\Delta\nu > 4.5 \times 10^5$ provides compelling evidence for a rapidly rotating neutron star in 4U 1636-53, and further supports the connection of burst oscillation frequencies with the spin frequencies of neutron stars. Our results provide further evidence that some millisecond pulsars are spun up via accretion in LMXBs. We also discuss the implications of our orbital velocity constraint for the masses of the components of 4U 1636-53.

Subject headings: Binaries: general - Stars: individual (4U 1636-53) - Stars: neutron - Stars: rotation - X-rays: stars - X-rays: bursts

1. Introduction

The low mass X-ray binary (LMXB) 4U 1636-53 is one of approximately 10 neutron star X-ray binaries which have revealed high frequency pulsations during thermonuclear bursts, hereafter "burst oscillations." The $\sim$ 581 Hz burst oscillations in 4U 1636-53 were discovered with the *Rossi X-ray Timing Explorer* (RXTE) by Zhang et al. (1997). These oscillations are almost certainly caused by rotational modulation of a nonuniform X-ray emission pattern on the neutron star surface. Near the onset of bursts this pattern likely takes the form of a hot spot (or possibly a pair of hot spots) induced on the neutron star surface by the ignition of nuclear burning (see Strohmayer, Zhang & Swank 1997). In the cooling part of the burst lightcurve the modulation pattern is less certain, but it may be induced by r-modes excited by the thermonuclear flash (see Heyl 2002), or perhaps "extreme weather," in the form of hydrodynamic vortices induced by thermonuclear heating (see Spitkovsky, Levin & Ushomirsky 2001). In particular, the large modulation amplitudes, high coherence and long term stability of the frequency are consistent with the rotation scenario (see Strohmayer et al. 1998a; Strohmayer & Markwardt 1999; Muno et al. 2000 and Giles et al. 2002).

To date there is only one known accreting millisecond X-ray pulsar, the 401 Hz pulsar SAX J1808-369 (Wijnands & van der Klis 1998; Morgan & Chakrabarty 1998). Several thermonuclear bursts have been observed from this source with the BeppoSAX Wide Field Cameras (in 't Zand et al. 1998). In the brightest of the three bursts seen from J1808-369 in 't Zand et al. (2001) found evidence for the presence of 401 Hz pulsations, providing additional support to the idea that burst oscillation frequencies are set by the spin frequencies of neutron stars.

Strohmayer et al. (1998b) suggested that observations of burst oscillations in bursts at different binary orbital phases might allow a determination of neutron star orbital velocities by measuring the orbital Doppler shifts in the burst oscillation frequency. Recently, Giles et al. (2002) have studied the distribution of the highest observed, or "asymptotic," oscillation frequencies in a large sample of bursts from 4U 1636-53. Their sample spans a time baseline of more than four years. They find a high degree of frequency stability over this timespan and attempt to constrain the neutron star orbital velocity using a portion of the observed asymptotic frequency distribution.

Over the last few years a new regime of nuclear burning on neutron stars has been revealed with the observation of very long (3 - 5 hr) thermonuclear bursts from six LMXBs (see Cornelisse et al. 2000; Strohmayer & Brown 2002; Wijnands 2001; Kuulkers et al. 2002; Cornelisse et al. 2002). These bursts likely result from unstable burning of the ashes, as for example, carbon, of hydrogen and/or helium burning (see Cumming & Bildsten 2001; Strohmayer & Brown 2001; Kuulkers 2001). Of the six superburst sources so far only 4U

1636-53 has produced more than one event. Strohmayer (see Strohmayer & Brown 2001) and Wijnands (2001) independently identified the superburst from 4U 1636-53 which ocurred on February 22, 2001; the former in pointed RXTE observations, the latter in the RXTE/ASM data. Using the ASM data Wijnands (2001) also identified a similar event from 4U 1636-53 which occurred 4.7 years earlier, thus providing the first constraint on the recurrence time for superbursts. Only two superbursts have been observed in detail with large area, high throughput instrumentation; a superburst from 4U 1820-30 (Strohmayer & Brown 2002), and the February 22, 2001 event from 4U 1636-53. Both were observed with the Proportional Counter Array (PCA) on board RXTE. Here we report the discovery of coherent pulsations at $\sim$ 582 Hz during the February 22, 2001 superburst from 4U 1636-53. The plan of this paper is as follows. In §1 we briefly describe the general properties of the superburst and the data available for high time resolution studies. We then discuss our discovery of $\sim$ 582 Hz pulsations and describe in detail the time evolution of the pulsation frequency and the expected behavior given the known binary orbital ephemeris for 4U 1636-53. In §3 we describe our phase coherent timing study and show that orbital modulation of the frequency fits the data extremely well and that the pulsation is coherent. We close in §4 with a summary and discussion of the implications of our findings. A detailed study of the spectral and energetics of this superburst will be presented in a future publication.

2. The February 22, 2001 Superburst

As part of an approved observing program for 4U 1636-53, RXTE observations were being conducted on February 22, 2001 when a several hour long superburst was observed. The 2-60 keV lightcurve of the superburst from Standard1 data is shown in Figure 1a with 1 second time resolution. The rise in count rate beginning near 5500 seconds in the figure represents the source coming out of Earth occultation. For several minutes after this the intensity level was about 4,800 counts/sec, significantly higher than the persistent source rate in the previous orbit, suggesting that the burst may have already begun within the Earth occultation gap. The sharp increase in count rate which follows is real and can be seen with 1/8 second resolution in Figure 1b. This part of the profile has a timescale characteristic of normal (10 - 20 s duration) type I bursts from 4U 1636-53, except that it shows an interesting double peaked structure. This behavior appears similar to that seen in the superburst from 4U 1820-30, which also showed a normal Type I burst temporal structure at its onset (see Figure 2 in Strohmayer & Brown 2002). Further study of these interesting aspects of the superburst will be described in a future publication.

During these observations data were sampled in two high time resolution modes, both

with a time resolution of 1/8192 seconds. The first was an event mode with 64 energy channels and the second a "burst catcher" mode designed to capture high time resolution lightcurves of bursts across the entire PCA bandpass. Our studies here were done with the event mode data. Due to the duration and intensity of the superburst, the telemetry rate was very high and RXTE's onboard data recorder, which operates in a "bucket" mode, was filled before it could be downloaded. Unfortunately some high time resolution data during the superburst were overwritten and lost. Standard mode data, such as shown in Figure 1 and which use much less telemetry capacity, are written to a different virtual channel in the data recorder and were therefore not overwritten. A similar circumstance ocurred when RXTE observed the superburst from 4U 1820-30 (see Strohmayer & Brown 2002). In spite of these difficulties, two intervals of high time resolution data were obtained; the first beginning just before the peak of the super burst, and the second in the decaying tail.

2.1. Detection of 581 Hz Pulsations

The first high time resolution data interval began at $\sim 17:00:44$ UTC on February 22, 2001 and lasted ~ 2500 seconds. We began our timing study by computing FFT power spectra of this interval. We used 1024 second intervals of the full 2 - 60 keV bandpass event mode data to compute two power spectra, each with a Nyquist frequency of 4096 Hz. We then searched these power spectra for significant signals in the vicinity of 581 Hz. It was clear almost immediately that the power spectrum of the first 1024 s interval contained a significant signal at ~ 581 Hz. The power spectrum of this interval, rebinned in frequency space by a factor of 8, is shown in Figure 2a and reveals a highly significant peak near 581 Hz. Figure 2b shows an expanded view of the region around 582 Hz, revealing a pair of peaks separated by ~ 0.03 Hz. The highest peak in this power spectrum has a single trial chance probability of $\sim 1 \times 10^{-21}$, so there is no doubt about the detection. The implied frequency width of ~ 0.03 Hz indicates a quality factor, $Q \equiv \nu_0/\Delta\nu > 19,400$, which without any additional timing analysis, is about a factor of 5 larger than that seen to date in burst oscillations from normal Type I bursts (see Strohmayer & Markwardt 1999; Muno et al. 2000). We did not detect a similar signal in the 2nd 1024 s data interval.

2.2. Time Evolution of the Pulsation Frequency

In order to investigate the time dependence of the pulsation frequency and to determine whether it persists throughout the entire interval we computed a dynamic power spectrum using the Z_1^2 power statistic (see Buccheri 1983; Strohmayer & Markwardt 1999). However, in

anticipation of the need for a precise timing analysis, we first barycentered the data using the standard RXTE software (faxbary) and planetary ephemerides (JPL-DE200). This analysis revealed that the two peaks in Figure 2 result from two segments of detectable pulsations during each of which the pulsation frequency is observed to increase in a roughly linear fashion. The $\sim$ 800 s interval which contains these two pulse trains is marked by the vertical dashed lines in Figure 1. Figure 3 shows a contour map of the dynamic Z_1^2 spectrum as well as the PCA countrate as a function of time. To produce Figure 3 we used 64 s intervals to compute Z_1^2 and we started a new interval every 16 s. This figure reveals a number of remarkable properties; first, the pulsations persist for *hundreds* of seconds, much longer than the $\sim$ 10 s pulse trains observed in normal bursts, and second, the overall frequency drift spans only about 0.04 Hz, which is very small compared with the $\sim$few Hz drifts observed in normal burst oscillations. The magnitude of this drift is similar to what could be produced solely by the Doppler motion of the neutron star in its binary orbit. A simple estimate, just using the observed magnitude of the frequency drift, would require $v_{ns} \sin i/c = \Delta\nu/\nu = 6.9 \times 10^{-5}$, which is equivalent to a velocity of $\sim$ 21 km s^{-1}. This suggests that we may be seeing a coherent pulsation modulated by orbital motion of the neutron star.

2.3. Expected Frequency Evolution Based on Binary Orbital Ephemeris

The $\sim$3.8 hr orbital period of V801 Arae, the optical companion to the neutron star in 4U 1636-53, is well known from optical observations. Recently, Giles et al. (2002) have used new optical observations to test and slightly modify the ephemeris determined from all historical optical observations by Augusteijn et al. (1998). Their resulting ephemeris: HJD = 2446667.3179(33) $\pm(N \times 0.15804693(16))$, predicts the epoch of maximum optical brightness in units of heliocentric Julian day. Although the formal statistical error in projecting this ephemeris forward to the time of the superburst is of order 4×10^{-4}, there is an $\sim$ 0.05 systematic phase uncertainty which results from the fact that the optical lightcurve does not have any sharp fiducial features and also has often shown night to night variations (see Giles et al. 2002 for a discussion).

We used this ephemeris to predict the orbital phase of the $\sim$ 800 s interval during the superburst which shows pulsations. The interval begins at MJD 51962.710160410, which corresponds to a phase of 0.352 relative to optical maximum (phase zero is optical maximum). One addtional piece of information is required to predict the corresponding frequency evolution, the relationship between the optical and dynamical ephemerides. For systems like 4U 1636-53, which show sinusoidal optical modulations and which have inclinations $\lesssim 60°$

the standard interpretation has been that optical maximum corresponds to superior conjunction of the optical secondary, that is, when the secondary is furthest from the observer. Figure 4 shows the predicted frequency behavior versus orbital phase of a coherent pulsation associated with the neutron star (as, for example, its spin frequency) given this relationship between the optical and dynamical phases. The predicted phase range of the superburst pulsation interval is denoted with vertical solid lines. The predicted frequency evolution is strikingly similar to that observed, moreover, even an uncertainty in the phase of ~ 0.1 would not change the qualitative conclusion that the frequency *should* be increasing because of the orbital motion. The original Augusteijn (1998) ephemeris predicts an orbital phase of 0.26 for the start of the oscillation interval. This is still in the range of orbital phases which would predict an increasing pulsation frequency. These considerations strongly suggest that the observed frequency variations are consistent with the orbital motion of the neutron star.

3. Phase Coherent Timing Analysis

In order to test the orbital modulation conclusion more quantitatively we performed coherent timing analyses using the complex Z_1 statistic (see Strohmayer & Markwardt 1998 for an example of the use of the Z_1^2 statistic in a similar context), where;

$$Z_1 = X + iY = \left(\sum_{j=1}^{N} \sin\phi_j\right) + i\left(\sum_{j=1}^{N} \cos\phi_j\right). \quad (1)$$

The Z_1^2 statistic is defined as $Z_1^2 = Z_1^* Z_1$, and the phase angle is given by $\psi = \tan^{-1}(Y/X)$. Here $\phi_j = 2\pi \int_0^{t_j} \nu(t')dt$, where $\nu(t')$ is the frequency as a function of time, and t_j are the observed X-ray event times.

3.1. Solution Using Total Z_1^2 Power

We used a circular orbit model to describe the time variation of the pulsation frequency and phase, *vis*;

$$\nu(t) = \nu_0 \left(1 - \frac{v_{ns} \sin i}{c} \sin(\omega_{orb} t + \phi_0)\right). \quad (2)$$

Here, ν_0, $v_{ns} \sin i/c$, ϕ_0 and ω_{orb} are the barycentric frequency, the projected neutron star velocity, the orbital phase at the start of the pulsation interval, and the orbital period, respectively. We used this model to predict the pulsation phase at time t and we varied the parameters in order to maximize Z_1^2. We used the data from the $\sim$ 800 s segment shown in Figure 3, but we excluded events in an $\sim$ 160 s segment between the two pulse trains in

which we did not detect significant pulsations. We fixed the orbital frequency ω_{orb}, since it is known with high precision and we cannot hope to constrain it further with such a short data segment, and we let ν_0, $v_{ns} \sin i/c$, and ϕ_0 vary. We began by making a grid search over a range of parameter space which produced, "by eye," reasonably plausible solutions. We then used a general function extremizer, TNMIN (see Nash 1984; implemented in IDL by C. M.), to optimize the solutions. We double checked the maximization using a simplex method (AMOEBA) implemented in FORTRAN. The two methods were in excellent agreement. We find that this model can describe the frequency and phase evolution very well. Our best fits have $Z_1^2 \approx 276$ which represents an enormous improvement compared to a model with no frequency evolution. We also compared the circular orbital model with a strictly linear increase of the frequency. The linear model achieves a maximum $Z_1^2 = 147$ showing that the orbit model performs significantly better. This is perhaps not too surprising given the additional parameters in the circular orbit model, however, the sense of the improvement is such that the frequency model with curvature (such that the frequency vs time curve is concave up) fit much better than linear models.

As the data segment is short compared to the 3.8 hour orbital period it is possible to find statistically similar solutions with a range of orbital parameters. Indeed, there is a broad ridge in Z_1^2 space on which the three parameters are strongly correlated. The best model in the sense of having the largest $Z_1^2 = 275$ has $\nu_0 = 582.1454$ Hz, $v_{ns} \sin i = 136$ km s^{-1} and $\phi_0 = 0.293$. However, models with $90 < v_{ns} \sin i < 175$ are not strongly excluded. A look at Figure 4 confirms why this is so. As long as the fitted orbital phase range is such that the curvature is concave up, then the other parameters, $v_{ns} \sin i/c$, and ν_0 can more or less adjust to approximate the observed frequency evolution.

Given the systematic uncertainty of order 0.05 in the optical phase and the additional uncertainty of the exact relationship between optical and dynamical phase it is not possibe to prefer *a priori* a particular ϕ_0, however, the range above is consistent with what is expected based on the optical ephemeris as long as optical maximum ocurrs within ~ 0.1 of superior conjunction of the secondary. These considerations show that the data can be well explained by a range of reasonable orbits, however, because of the shortness of the pulse train we cannot place tighter constraints on the orbital parameters using these data alone. Nevertheless the observed pulsations are highly coherent as we are able to track $\sim 500,000$ consecutive cycles.

In Figure 5 we compare the standard FFT power spectrum with the Z_1^2 power spectrum using our best orbital parameters. The pair of weak broad peaks near 581.91 Hz are from the standard FFT analysis and are effectively the same as the pair of peaks in Figure 2. The narrow peaks near 582.1 Hz come from the Z_1^2 spectrum and result from the coherent addition of the two pulse trains. The nearby aliased peaks are caused by the need to bridge

the gap between the two pulse trains. Figure 6 shows the best orbital frequency model plotted over the dynamic Z_1^2 contours, and demonstrates visually that it track the frequency vs time contours very well. The success of the coherent timing analysis provides strong evidence that we are seeing the orbital modulation of coherent pulsations during the superburst.

3.2. Phase Evolution Analysis

Using this method we can also investigate the problem in the context of phase evolution as a function of time. For a given set of model parameters we can compute the phase, ϕ_j, of each x-ray event. We can then break up the full set of events into a set of M bins and compute the phase ψ_k for each bin. The phases are simply given by;

$$\psi_k = \tan^{-1}\left(\sum_m \cos\phi_m / \sum_m \sin\phi_m\right) \quad , \tag{3}$$

where the index m runs over all events in bin k. We can then compute $\chi^2 = \sum_{k=1}^{M} \left(\psi_k - \psi_{avg}\right)^2 / \sigma_{\psi_k}^2$, where ψ_{avg} is the average phase angle computed from all M bins. We can then minimize χ^2 to find a best fitting model. For a coherent signal the error σ_{ψ_k} in the phase angle is given simply by $1/\sqrt{(Z_1^2)}$, a result which we have confirmed with monte carlo simulations. This procedure is essentially equivalent to the phase connected timing analysis of burst oscillations described by Muno et al. (2000).

To further explore the phase coherence of our orbital solutions we broke up our event data into 24 segments and carried out the χ^2 minimization described above. We found that the best orbit model was entirely consistent with the model obtained from maximizing the Z_1^2 statistic. The minimum χ^2 was 23.3, which for 20 degrees of freedom (3 parameters and 1 additional degree of freedom from calculating ψ_{avg}) gives a statistically acceptable solution. The resulting phase residuals and errors are shown in Figure 7 in units of milliperiods. The rms level of ~ 46 milliperiods is indicated by the dashed horizontal lines. This is equivalent to ~ 79 μs. Although the residuals are unstructured in the sense they do not show any large systematic deviations, there is some weak evidence for phase "wobbling" (or timing noise in the parlance of radio pulsar timing) with a scale of about $20 - 40$ milliperiods on timescales of ~hundreds of seconds, particularly during the first pulse train. Such wobbling is also suggested by dynamic power spectral and phase coherent studies of some burst oscillations (see for example, Wijnands, Strohmayer & Franco 2000; Muno, Chakrabarty & Galloway 2002). To find the 90% confidence limits on the model parameters we found where $\Delta\chi^2 = 6.25$, which is appropriate for a 3 parameter fit. This gives a 90% confidence range for each orbit parameter of; $582.0390 < \nu_0$ (Hz) < 582.2262, $90 < v_{ns} \sin i$ (km s^{-1}) < 175, and $0.336 > \phi_0 > 0.277$.

We next used our best timing solution to phase fold the data and obtain an average pulse profile which we show in Figure 8. The units are counts and we repeat 2 cycles for clarity. The pulse profile is consistent with a sinusoid with an amplitude (expressed as its half amplitude) of 1% of the mean. Having computed a coherent solution we also made a sensitive search for harmonics and subharmonics, but we did not detect any higher harmonics nor the $\sim$ 290 Hz subharmonic (see Strohmayer & Markwardt 1999; Miller 1999; Strohmayer 2001). The 90% confidence uppers limits to the signal amplitude at the 290 Hz subharmonic and 1,160 Hz 1st harmonic are 0.1 and 0.06%, respectively.

4. Implications and Discussion

The discovery of coherent pulsations during a superburst from 4U 1636-53 has many interesting implications and also raises many questions. First, the observation of coherent pulsations from 4U 1636-53 confirms the presence of a rapidly rotating neutron star in 4U 1636-53. For example, our observation of $\sim 500,000$ pulsation cycles at 582 Hz is roughly analogous to observing a standard $\sim$ 1 s period radio or X-ray pulsar for $\sim$ 6 days. There would seem to be little doubt that such stability can only reflect the spin period of the neutron star.

4.1. Implications for Burst Oscillations

Our coherent timing analysis places a constraint on the barycentric frequency of the coherent pulsation in 4U 1636-53 of $582.0390 < \nu_0 < 582.2262$ Hz. This range is higher than any of the asymptotic burst oscillation frequencies measured for 4U 1636-53 by Giles et al. (2002). Our 90% upper limit is about 0.4 Hz above the highest asymptotic oscillation frequency (see Giles et al. 2002), but the limits on the barycentric pulsar frequency are reasonably consistent with the *total* observed spread around this peak (see Figure 6 in Giles et al. 2002). The fact that the implied pulsar frequency is within $\sim$1 Hz of all the measured asymptotic frequencies provides further evidence that the frequencies observed during the more numerous, short duration ($\sim$ 10 s) thermonuclear bursts are indeed set by the rotational frequency of the neutron star. However, since the distribution of *all* asymptotic burst oscillation periods from 4U 1636-53 are not strongly correlated with orbital phase there arguably must be an additional source of variation in the asymptotic frequencies of burst oscillations above that caused by orbital motion of the neutron star.

There has been much recent theoretical work to provide an explanation of the $\sim$few Hz

frequency drifts observed in burst oscillations. For example, Cumming et al. (2002) have reevaluated their earlier (Cumming & Bildsten 2000) theoretical calculations of spin down in the neutron star surface layers produced by hydrostatic expansion and angular momentum conservation during thermonuclear bursts. They conclude that such expansion alone is probably not capable of accounting for the largest observed frequency drifts. More recently, Spitkovsky, Levin & Ushomirsky (2002) have investigated the effects of burst heating in the atmosphere and show that this can drive strong zonal flows which can also produce frequency drifts. They suggest that some combination of radial uplift and horizontal flows may explain the observed drift. Heyl (2002) has recently proposed that r-modes excited by the thermonuclear burst may be responsible for producing the observed modulation, especially in the decaying tails, and that the motions of these waves relative to the star can produce the observed frequency drifts.

Our results provide further impetus for such work. The discovery of coherent pulsations argues compellingly for the spin interpretation, which can be summarized as follows. The observed modulations are caused by the rotation of some anisotropic emission pattern on the neutron star surface. Near burst onset the pattern is most likely a localized "spot" (or perhaps anitpodal spots). At late times in the burst tails it may be produced by an oscillation mode, perhaps the r-modes suggested by Heyl (2002), or the hydrodynamic vortices proposed by Spitkovsky, Levin & Ushomirsky (2002). However, the observed frequency drifts and variations in the asymptotic burst frequencies must be accomodated within a succesful model. It seems most likely that the observed frequency drifts result from the fact that the emission pattern is not fixed in the rotating frame of the neutron star. Oscillation modes, as for example the r-modes, are not fixed in the rotating frame, and thermonuclear flame fronts can move across the surface of the star. In addition, thermonuclear heating drives both radial and horizontal motions, both of which may contribute to the $\lesssim 1\%$ frequency drifts.

4.2. What Causes the Flux Modulation?

The coherent pulsations observed during the superburst have an average amplitude $\sim 1\%$, smaller than is typical for burst oscillations from normal bursts. This raises the interesting question; what causes the flux modulations during the superburst and how does it relate to that which operates during normal bursts? If a weak coherent modulation were always present with some fixed amplitude, then if the source intensity increased–as during the superburst–the modulation could become detectable. This seems unlikely, however, since there are intervals during the burst at roughly similar intensities which do not show detectable pulsations. More likely, there is some intrinsic change in the modulation amplitude

caused by the superburst. There is good evidence that these events result from the release of thermonuclear energy at great depth ($\sim 10^{13}$ g cm^{-2}, see Strohmayer & Brown 2002; Cumming & Bildsten 2001). If the energy release and/or transport is anisotropic then a flux asymmetry at the surface could be produced. Alternatively, the burst flux might excite an oscillation mode (as, for example, suggested by Heyl 2002). In either case, if such a process produced a weak $\sim 1\%$ modulation which varied in strength by about a factor of two, then the intervals of strongest modulation would be detectable, but because the spectral power varies as the square of the modulation amplitude, a modest drop in the amplitude would render the modulation undetectable. Alternatively, variable photon scattering in the vicinity of the neutron star could also change the modulation amplitude. Further insight into these issues could result from a phase resolved spectral study, which we will pursue in subsequent work.

4.3. Constraints on the Component Masses

Our coherent timing analysis places a constraint on the projected neutron star velocity. As mentioned above, a range of orbital velocities, initial phases and pulsar frequencies are allowed by the data. Giles et al. (2002) used the observed distribution of asymptotic burst oscillation frequencies to constrain the neutron star velocity. They obtained a 99% upper limit on $v_{ns} \sin i = 50$ km s^{-1} using a subset of 18 bursts which showed a tight clustering in asymptotic frequency. Although our inferred velocity range is outside their limit, the difference may reflect the exclusion of some bursts from the analysis by Giles et al. (2002). Indeed, the overall spread in frequency of *all* the bursts from 4U 1636-53 is not strongly at odds with the higher neutron star velocity inferred from our timing analysis here (see for example Figure 6 in Giles et al. 2002). This does suggest, however, that it will likely be even more difficult to infer reliable neutron star orbital velocities using normal burst oscillation frequencies than indicated by the Giles et al. (2002) study.

A measurement of the neutron star orbital velocity has implications for the masses of the binary components in 4U 1636-53. Although the system inclination is not precisely known, the lack of both eclipses and dips suggests that it cannot be much greater than $\sim 60°$ (see for example, Frank et al. 1987). Figure 9 shows the range of allowable masses for the components, with the secondary mass along the abscissa and the neutron star mass along the ordinate. Velocity contours are shown for the limits calculated from our orbital timing solutions. Contours are drawn for two inclinations, 70° (dashed) and 60° (solid). The allowed masses are those enclosed by the velocity contours. If the secondary were a main sequence star which fills its Roche lobe, then its mass is predicted to be $\sim 0.36 M_{\odot}$ (see

Smale & Mukai 1988: Patterson 1984). As can be seen a neutron star mass of $1.4M_{\odot}$ and a secondary mass of $0.36M_{\odot}$ are barely consistent with our derived limits, suggesting that the secondary may be more massive than simple estimates would indicate.

REFERENCES

Augusteijn, T., van der Hooft, F., de Jong, J.A., van Kerkwijk, M.H., & van Paradijs, J., 1998, A&A, 332, 561

Buccheri, R. et al. 1983, A&A, 128, 245

Chakrabarty, D. & Morgan, E. H. 1998, Nature, 394, 346

Cornelisse, R., Kuulkers, E., in't Zand, J. J. M., Verbunt, F. & Heise, J., 2002, A&A, 382, 174

Cornelisse, R., Heise, J., Kuulkers, E., Verbunt, F., & in't Zand, J. J. M. 2000, ApJ, 357, L21

Cumming, A. & Bildsten, L. 2000, ApJ, 544, 453

Cumming, A. et al. 2001, ApJ, submitted, (astro-ph/0108009)

Frank, J., King, A. R. & Lasota, J.-P. 1987, A&A, 178, 137

Giles, A.B., Hill, K.M., Strohmayer, T. E. & Cummings, N. 2002, ApJ, 568, 222

Heyl, J. S. 2001, astro-ph/0108450

in 't Zand, J. J. M. et al. 1998, A&A, 331, L25

in 't Zand, J. J. M. et al. 2001, A&A, 372, 916

Kuulkers, E. 2001, The Astronomers Telegram, #68, 68, 1

Kuulkers, E. et al. 2002, A&A, 382, 503

Miller, M. C. 1999, ApJ, 515, L77

Morgan, E. H. & Chakrabarty, D. 1998, Nature, 394, 346

Muno, M. P., Fox, D. W., Morgan, E. H. & Bildsten, L. 2000, ApJ, 542, 1016

Nash, S. G. 1984, SIAM J. Num. Anal., 21, 770

Patterson, J. 1984, ApJS, 54, 443

Smale, A. P. & Mukai, K. 1988, MNRAS, 231, 663

Spitkovsky, A., Levin, Y. & Ushomirsky, G. 2001, ApJ, 566, 1018

Strohmayer, T. E. & Brown, E. F. 2002, ApJ, 566, 1045

Strohmayer, T. E. 2001, Advances Sp. Res., vol. 28, Nos 2-3, 511

Strohmayer, T.E., Zhang, W., & Swank, J.H., 1997, ApJ, 487, L77

Strohmayer, T. E., Zhang, W., Swank, J. H., White, N. E. & Lapidus, I. 1998a, ApJ, 498, L135

Strohmayer, T.E., Zhang, W., Swank, J.H., & Lapidus, I., 1998b, ApJ, 503, L147

Strohmayer, T.E., & Markwardt, C.B., 1999, ApJ, 516, L81

Wijnands , R. 2001, ApJ, 554, L59

Wijnands, R., & van der Klis, M. 1998, Nature, 394, 344

Zhang, W. W., Lapidus, I., Swank, J. H., White, N. E. & Titarchuk, L. 1997, IAUC, 6541

This preprint was prepared with the AAS LaTeX macros v5.0.

Figure Captions

Fig. 1.— Lightcurve of the superburst from 4U 1636-53 observed on February 22, 2001 (top). The data are the 2 - 60 keV PCA countrates from the Standard1 datamode. In the top panel the time resolution is 1 s. The dashed vertical lines denote the $\sim$ 800 s interval in which pulsations are detected. An exploded view of the sharp rise near the start of the burst is also shown (bottom). Here the time resolution is 1/8 s. Note the double peaked profile which shows timescales typically seen in normal Type I X-ray bursts ($\sim$ 10 s).

Fig. 2.— Power spectrum (top) of the first 1024 second data interval starting at 17:00:44 UTC. The spectrum was computed using the full bandpass event mode data. The Nyquist frequency is 4096 Hz. The frequency resolution is 1/128 Hz. The significant peak near 581 Hz is evident. An expanded view of the region around 582 Hz is also shown (bottom). The frequency resolution in this plot is 1/256 Hz. Two peaks separated by $\sim$ 0.03 Hz are clearly resolved.

Fig. 3.— Dynamic Z_1^2 power spectrum of the 800 s interval containing significant pulsations. The Z_1^2 data were computed using 64 s data intervals and a new interval was started every 16 s. Contours at 16, 18, 20, 22, 25, 30, 35, 40, 45, 50, 60, 70, 80, and 90 are shown. Two pulse trains are clearly evident, separated by a gap of $\sim$ 200 seconds. The PCA countrate (4 detectors) is also shown (see right axes).

Fig. 4.— Predicted orbital frequency evolution of a coherent pulsation centered on the neutron star in 4U 1636-53 and the orbital phase range of the 800 second pulsation interval during the superburst. We used the optical ephemeris from Giles et al. (2002) along with the single assumption that optical maximum corresponds to superior conjunction of the optical secondary. The vertical lines denote the phase range of the 800 s pulsation interval. The curve shows the frequency modulation which would be produced with $v \sin i = 62$ km s^{-1} for the neutron star. This is not intended to represent a fit to the observed frequency evolution, but rather to simply show the qualitative nature of the predicted frequency evolution. Even with an offset of the phase relationship between optical max and superior conjunction of $\sim$ 0.1 the ephemeris predicts that a pulsation frequency associated with the neutron star should be increasing.

Fig. 5.— Comparison of the FFT power spectrum which assumes no frequency or phase evolution with the Z_1^2 power spectrum computed using the best orbital frequency evolution model. The weak, broad peaks to the left of the figure are from the standard FFT power spectrum, while the sharp peaks to the right result from the phase coherent Z_1^2 power spectrum. The multiple (aliased) peaks in the coherent spectrum result from the gap between the two pulse trains.

Fig. 6.— Dynamic Z_1^2 contours as a function of frequency and time. Also shown is the frequency evolution from the best orbit model. The solid curve shows the model with $\nu_0 =$ 582.1454 Hz, $v_{ns} \sin i = 136$ km s^{-1} and $\phi_{dyn} = 0.293$ and has a $Z_1^2 = 275.5$. Note how the model tracks the observed frequency evolution very well.

Fig. 7.— Pulse phase residuals (observed - model) for our best fitting orbit model. The units are milliperiods. The rms deviation is ~ 46 milliperiods and is denoted by the dashed horizontal lines. There is some modest indication of an additional phase "wobbling" in the first pulse train.

Fig. 8.— Average pulse profile in the full 2 - 60 keV band produced by folding the two observed pulse trains with the best fitting orbit model. The profile is sinusoidal and has an amplitude of 1%.

Fig. 9.— Allowable component masses for 4U 1636-53 inferred from the neutron star orbital velocity constraints. A pair of velocity limits are plotted for two representative orbital inclinations, 60° (solid), and 70° (dashed). The curves are labelled with the respective velocity.

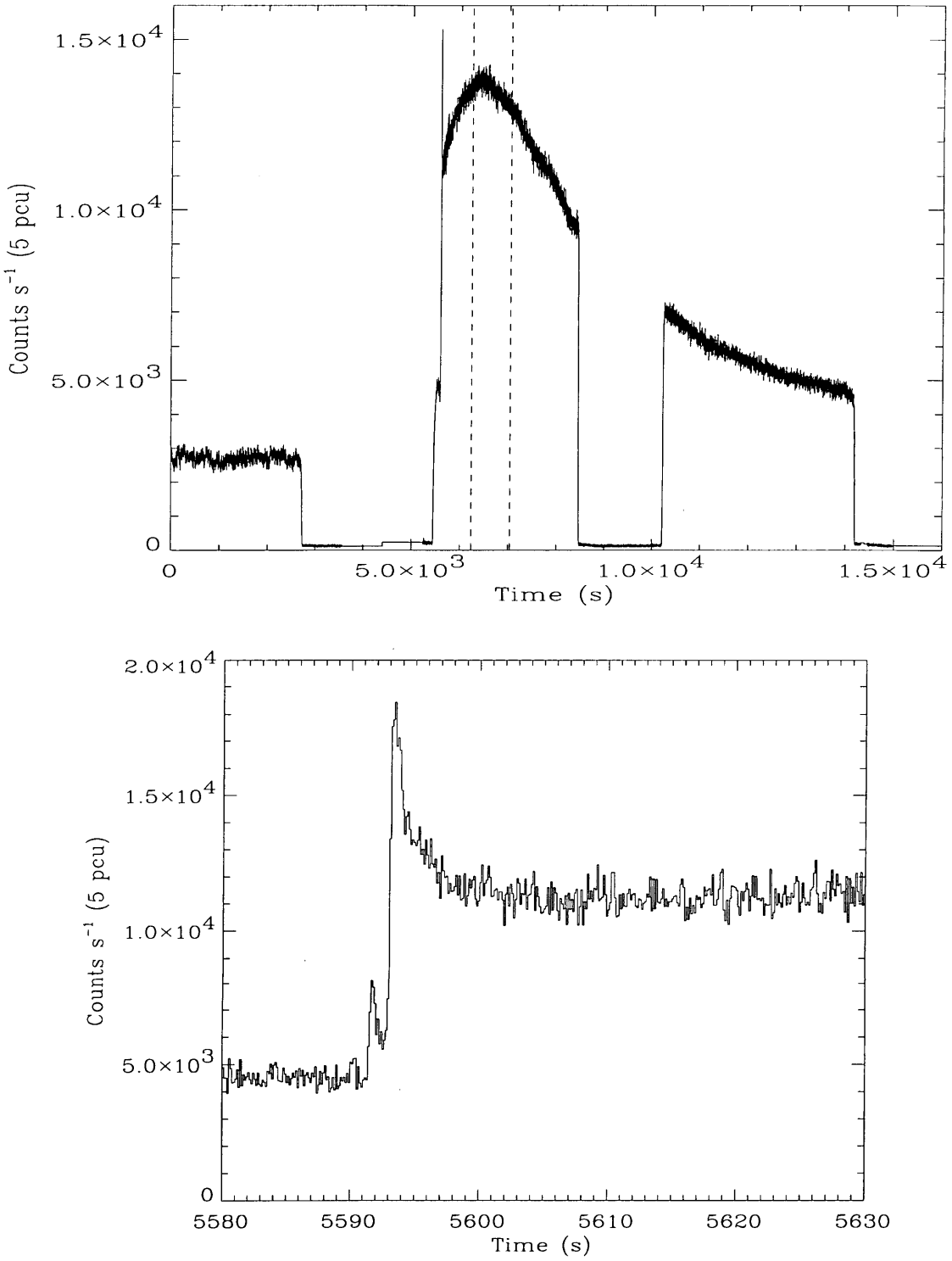

Figure 1: Lightcurve of the superburst from 4U 1636-53 observed on February 22, 2001 (top). The data are the 2 - 60 keV PCA countrates from the Standard1 datamode. In the top panel the time resolution is 1 s. The dashed vertical lines denote the $\sim$ 800 s interval in which pulsations are detected. An exploded view of the sharp rise near the start of the burst is also shown (bottom). Here the time resolution is 1/8 s. Note the double peaked profile which shows timescales typically seen in normal Type I X-ray bursts ($\sim$ 10 s).

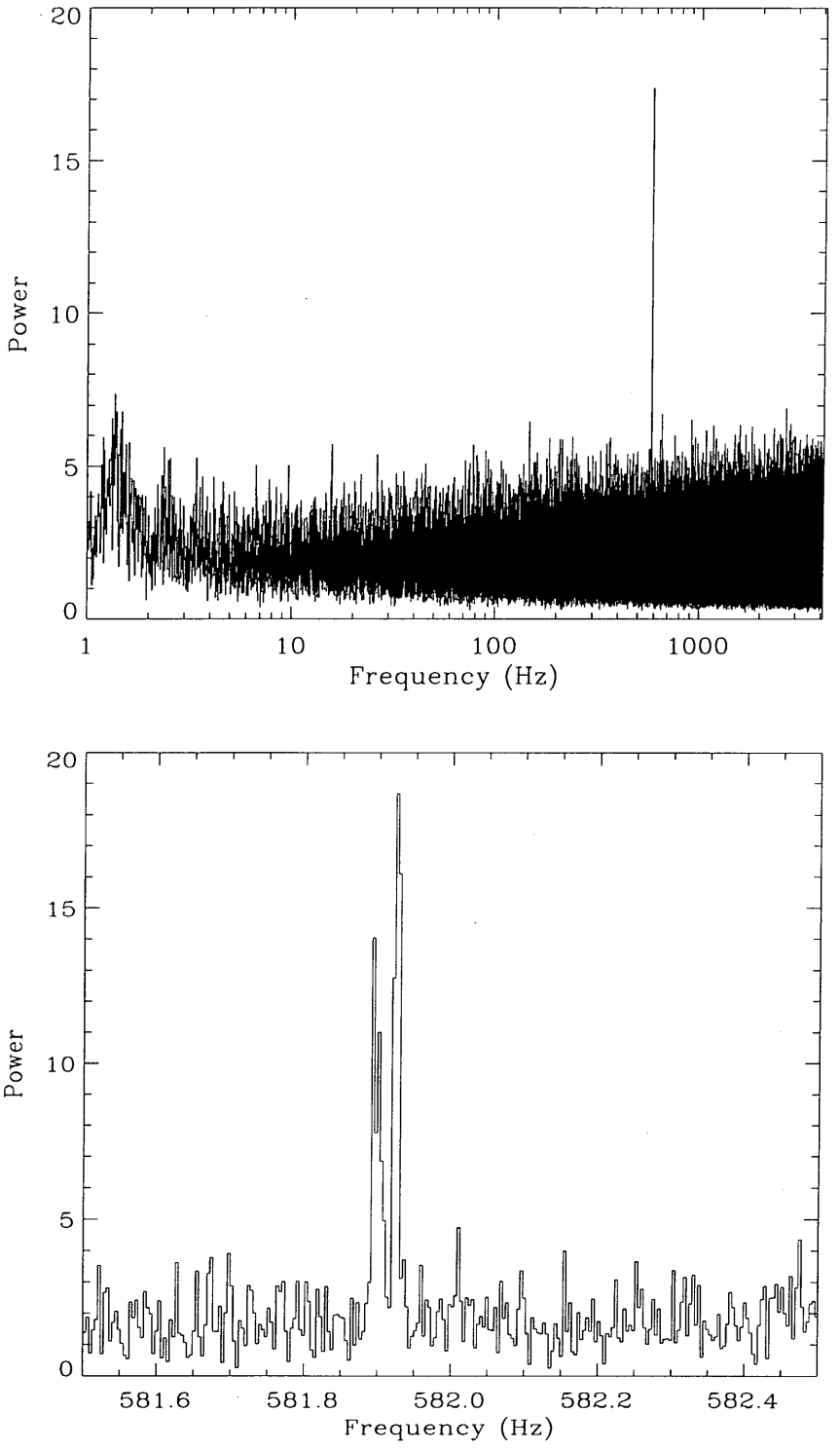

Figure 2: Power spectrum (top) of the first 1024 second data interval starting at 17:00:44 UTC. The spectrum was computed using the full bandpass event mode data. The Nyquist frequency is 4096 Hz. The frequency resolution is 1/128 Hz. The significant peak near 581 Hz is evident. An expanded view of the region around 582 Hz is also shown (bottom). The frequency resolution in this plot is 1/256 Hz. Two peaks separated by ~ 0.03 Hz are clearly resolved.

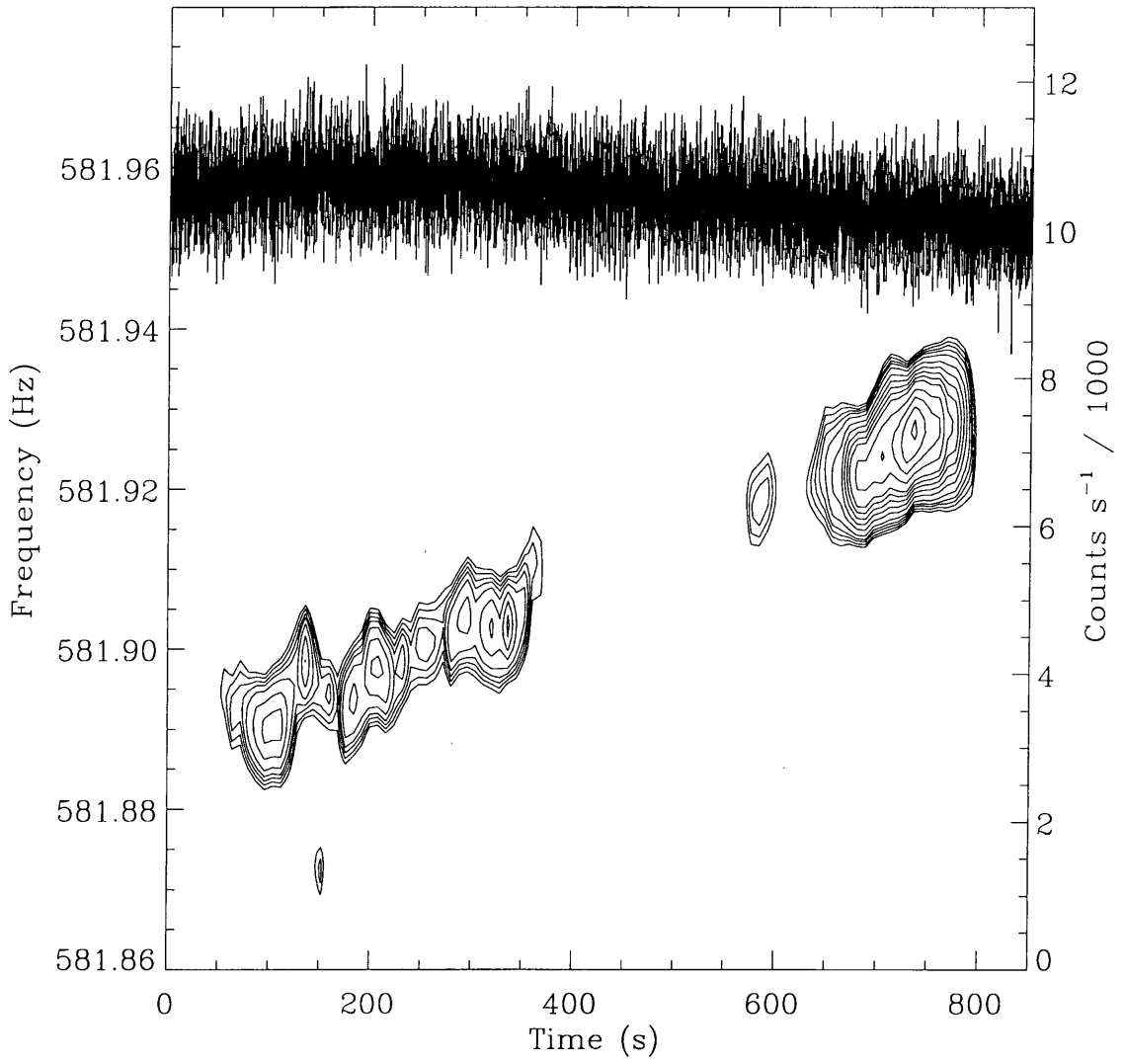

Figure 3: Dynamic Z_1^2 power spectrum of the 800 s interval containing significant pulsations. The Z_1^2 data were computed using 64 s data intervals and a new interval was started every 16 s. Contours at 16, 18, 20, 22, 25, 30, 35, 40, 45, 50, 60, 70, 80, and 90 are shown. Two pulse trains are clearly evident, separated by a gap of $\sim$ 200 seconds. The PCA countrate (4 detectors) is also shown (see right axes).

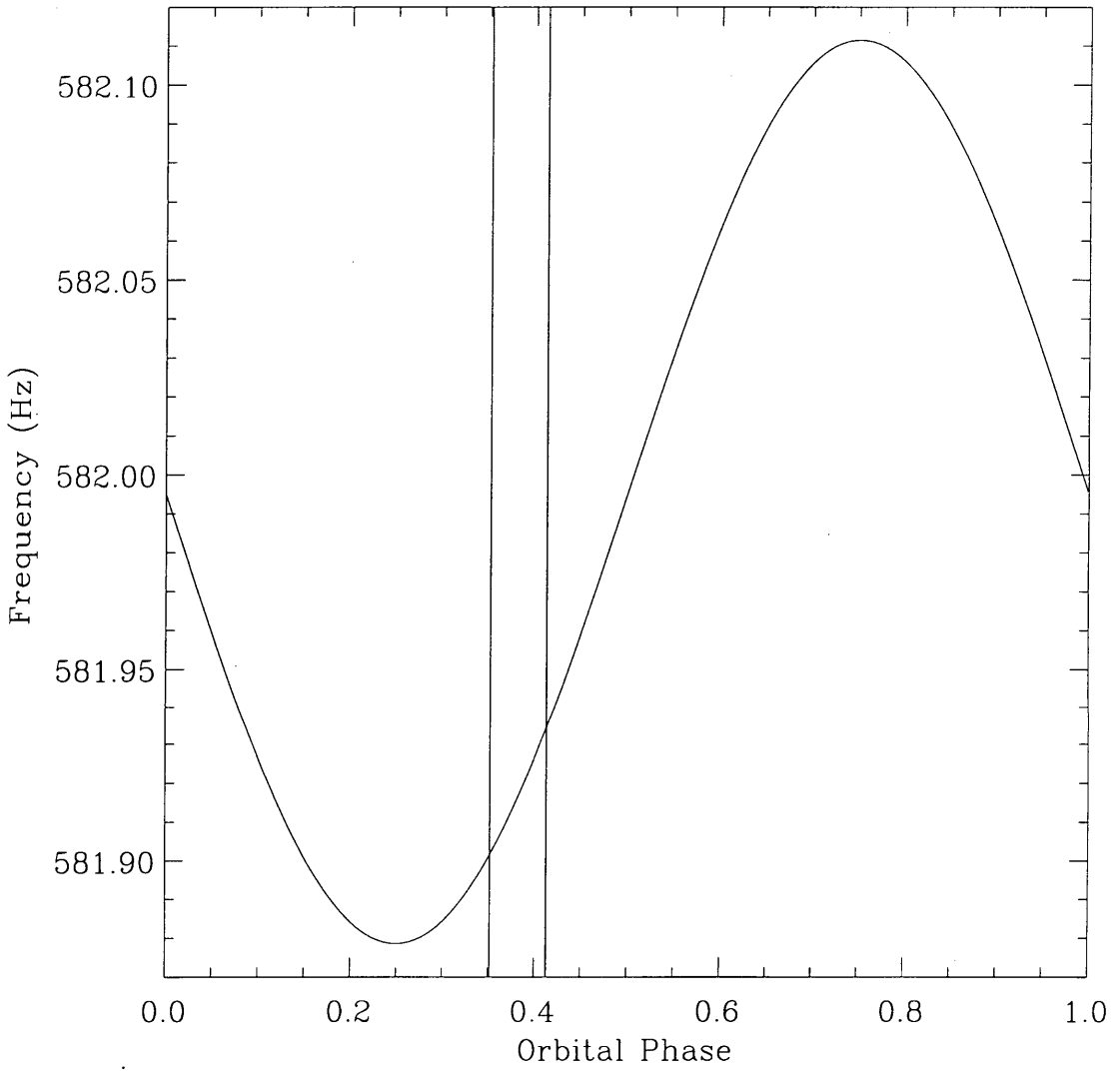

Figure 4: Predicted orbital frequency evolution of a coherent pulsation centered on the neutron star in 4U 1636-53 and the orbital phase range of the 800 second pulsation interval during the superburst. We used the optical ephemeris from Giles et al. (2002) along with the single assumption that optical maximum corresponds to superior conjunction of the optical secondary. The vertical lines denote the phase range of the 800 s pulsation interval. The curve shows the frequency modulation which would be produced with $v \sin i = 62$ km s^{-1} for the neutron star. This is not intended to represent a fit to the observed frequency evolution, but rather to simply show the qualitative nature of the predicted frequency evolution. Even with an offset of the phase relationship between optical max and superior conjunction of ~ 0.1 the ephemeris predicts that a pulsation frequency associated with the neutron star should be increasing.

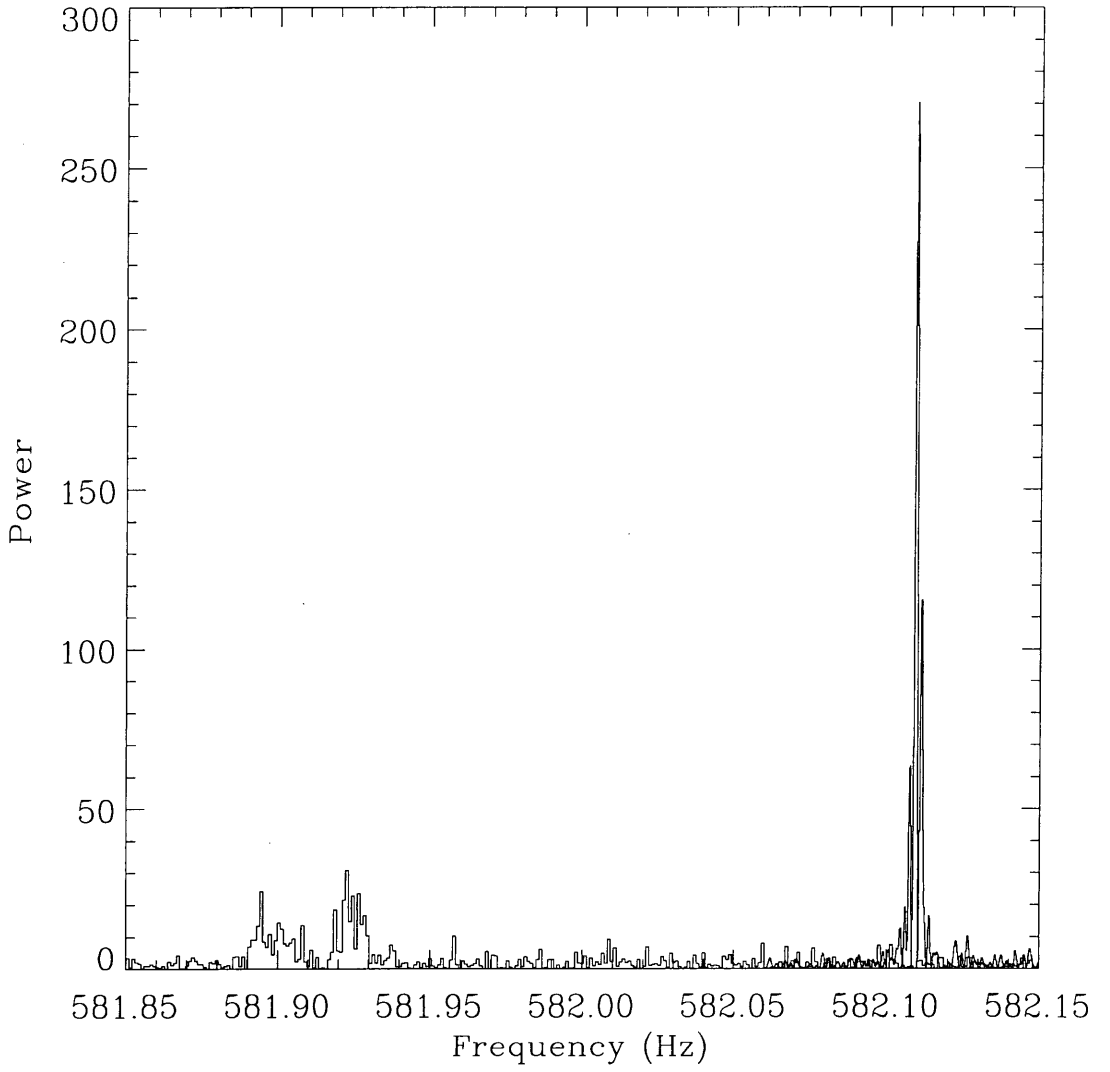

Figure 5: Comparison of the FFT power spectrum which assumes no frequency or phase evolution with the Z_1^2 power spectrum computed using the best orbital frequency evolution model. The weak, broad peaks to the left of the figure are from the standard FFT power spectrum, while the sharp peaks to the right result from the phase coherent Z_1^2 power spectrum. The multiple (aliased) peaks in the coherent spectrum result from the gap between the two pulse trains.

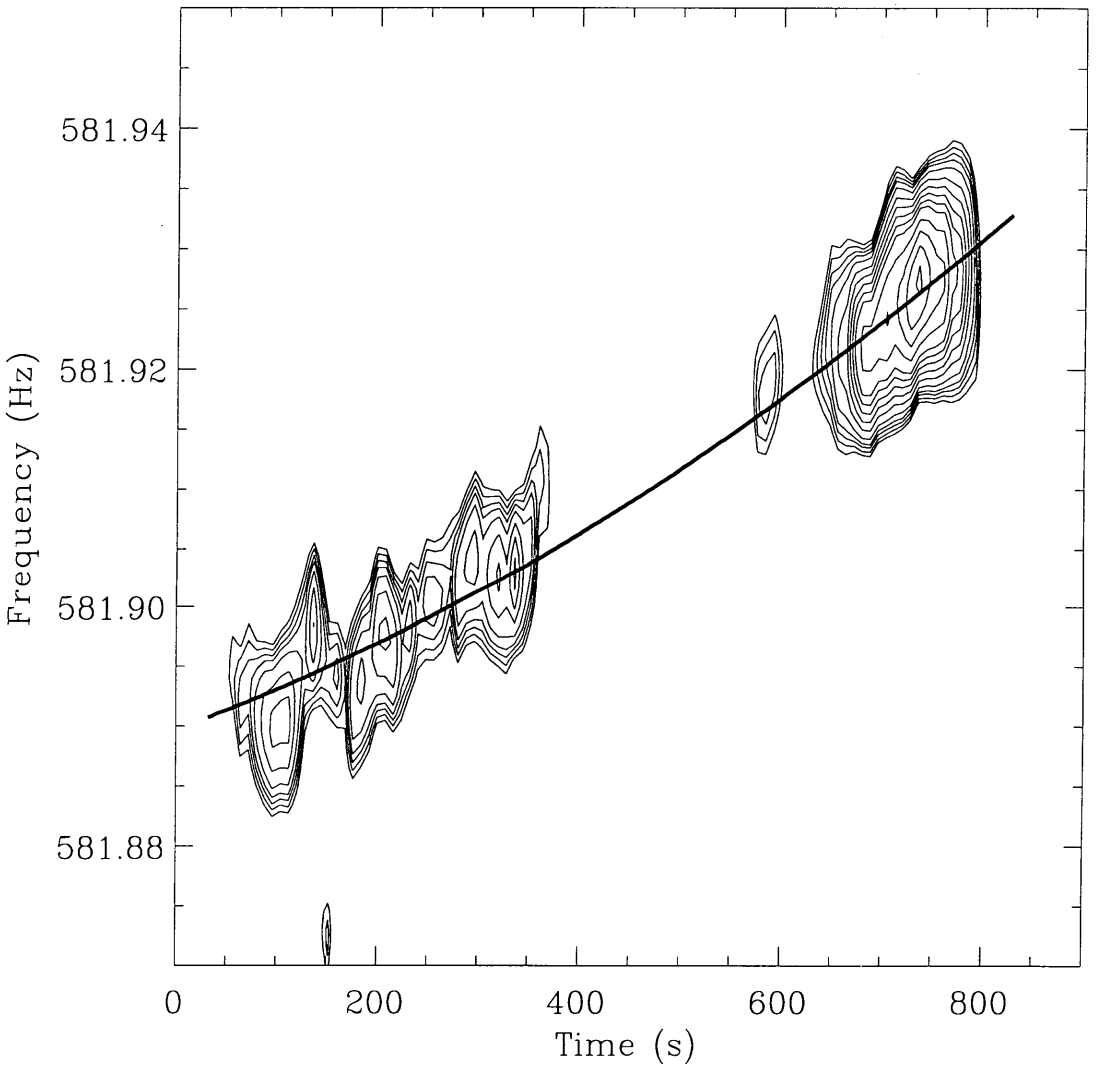

Figure 6: Dynamic Z_1^2 contours as a function of frequency and time. Also shown is the frequency evolution from the best orbit model. The solid curve shows the model with $\nu_0 =$ 582.1454 Hz, $v_{ns} \sin i = 136$ km s^{-1} and $\phi_{dyn} = 0.293$ and has a $Z_1^2 = 275.5$. Note how the model tracks the observed frequency evolution very well.

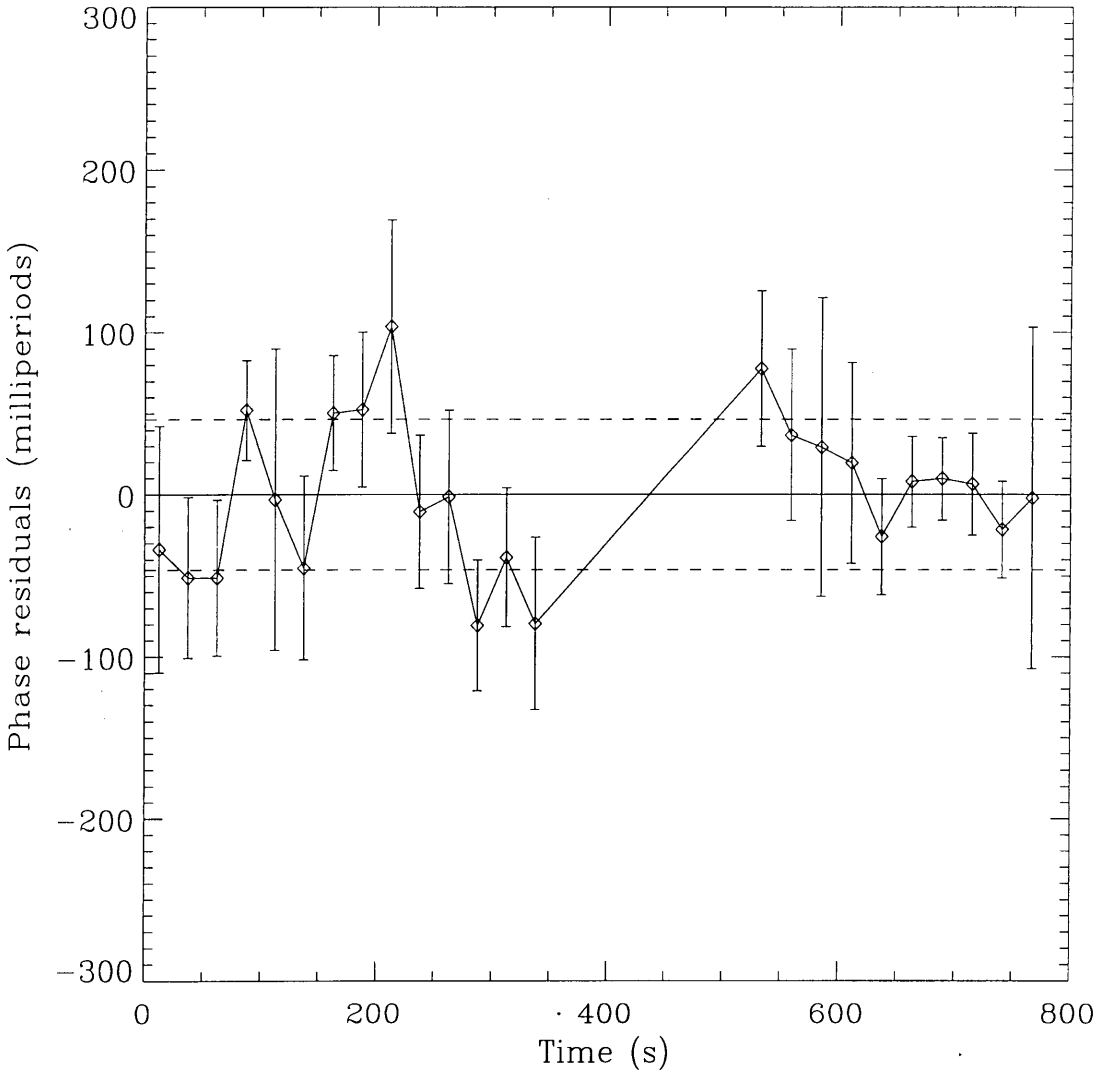

Figure 7: Pulse phase residuals (observed - model) for our best fitting orbit model. The units are milliperiods. The rms deviation is ~ 46 milliperiods and is denoted by the dashed horizontal lines. There is some modest indication of an additional phase "wobbling" in the first pulse train.

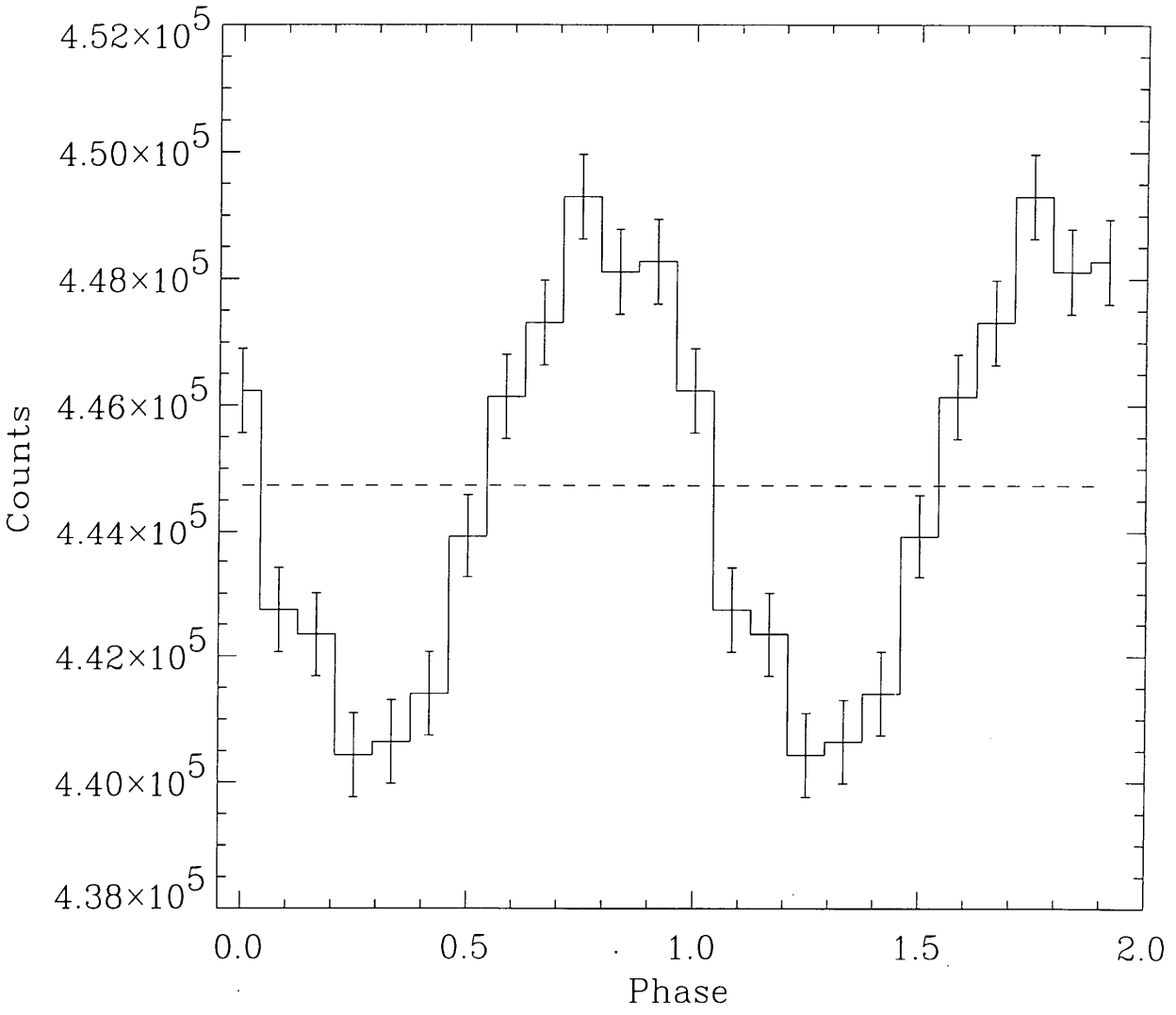

Figure 8: Average pulse profile in the full 2 - 60 keV band produced by folding the two observed pulse trains with the best fitting orbit model. The profile is sinusoidal and has an amplitude of 1%.

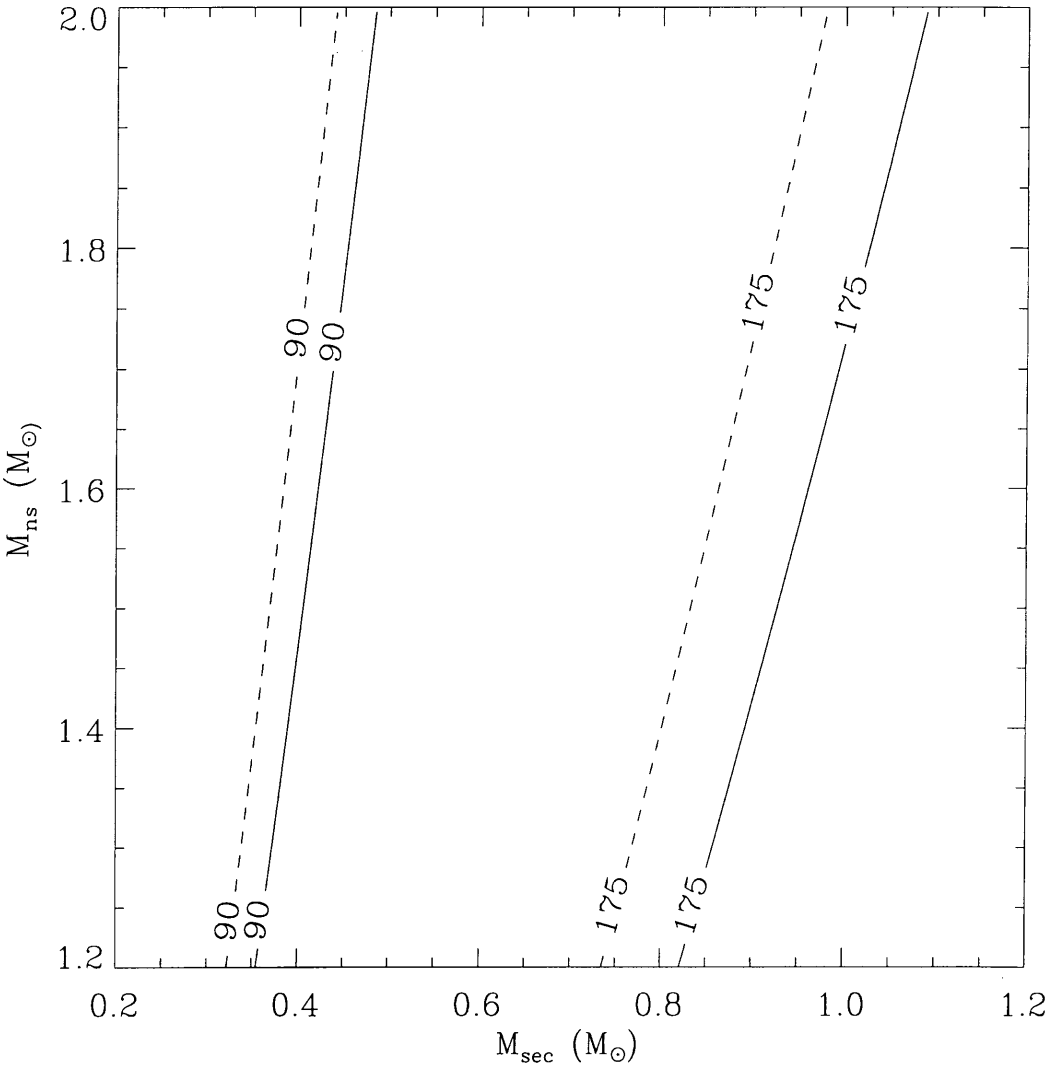

Figure 9: Allowable component masses for 4U 1636-53 inferred from the neutron star orbital velocity constraints. A pair of velocity limits are plotted for two representative orbital inclinations, 60° (solid), and 70° (dashed). The curves are labelled with the respective velocity.